INDONESIAN JOURNAL ON GEOSCIENCE
Geological Agency
Ministry of Energy and Mineral Resources

Journal homepage: http://ijog.geologi.esdm.go.id
ISSN 2355-9314, e-ISSN 2355-9306

Characterizing SO_2 Emission Rate, Thermal Anomalies, from Opened and Closed Vent System at Agung, Bromo, and Sinabung Volcanoes in Indonesia

Hilma Alfianti[1], Asep Saepuloh[2], Mamay Surmayadi[1], Syegi L. Kunrat[1], Ugan B. Saing[1], I.G.B. Eddy Sucipta[2], and Sofyan Primulyana[1]

[1]Centre for Volcanology and Geological Hazard Mitigation, Geological Agency, Ministry of Energy and Mineral Resources, Bandung, Indonesia
[2]Faculty of Earth Sciences and Technology, Bandung Institute of Technology, Bandung, Indonesia

Corresponding author: saepuloh@itb.ac.id
Manuscript received: November 20, 2021; revised: June 14, 2022;
approved: November 20, 2023; available online: August, 18, 2023

Abstract - Agung, Bromo, and Sinabung Volcanoes have high volcanic activity over the last decade, and have different eruption characteristics. Hence, it would be fascinating to study the characteristics of their volcanic activity patterns based on SO_2 emission rates and thermal anomaly correlated with the seismicity data. The SO_2 emission rate measurement was carried out using the Differential Optical Absorption Spectroscopy (DOAS), and calculated based on SO_2 column density, distance of measurement, wind speed, and wind direction. In addition, SO_2 emission was detected using Ozone Monitoring Instrument (OMI) images with daily global coverage. Thermal anomaly detection was performed using Advance Spaceborne Thermal Emission and Reflection Radiometer (ASTER) of Thermal Infrared (TIR) subsystem with high spatial resolution (90x90 m). ASTER TIR images were corrected for radiometric and thermal atmospheric. The emissivity and brightness temperature separation algorithm was applied to obtain surface temperature of Agung, Bromo, and Sinabung Volcanoes. All the data were correlated with the seismicity of each volcano. The SO_2 emission rates correlate with the magma ascent to the shallow depth in an open system volcano (Bromo Volcano). In the closed-system volcanoes (early phase of Agung and Sinabung), SO_2 emission was detected after the transition of closed to open system. Magmatic injection from the reservoir to the shallow depth was detected as thermal anomalies, such as in Agung Volcano. Whereas in Bromo Volcano, the thermal anomaly was insignificant since Bromo Volcano has an explosive eruption at a short period, so the ASTER image could not observe the thermal anomaly on the eruption time. Thermal anomaly pattern in Sinabung Volcano was the manifestation of new magmatic injection to the shallow depth. Therefore, their increase serves as indicators for the increasing magmatic activity prior to the eruptions.

Keywords: SO_2 emission rate, thermal anomaly, DOAS, OMI, ASTER, Open Vent, Closed Vent

© IJOG - 2023

How to cite this article:
Alfianti, H., Saepuloh, A., Surmayadi, M., Kunrat, S.L., Saing, U.B., Sucipta, I.G.B.E., and Primulyana,S., 2023. Characterizing SO_2 Emission Rate, Thermal Anomalies, from Opened and Closed Vent System at Agung, Bromo, and Sinabung Volcanoes in Indonesia. *Indonesian Journal on Geoscience*, 10 (2), p.277-295. DOI: 10.17014/ijog.10.2.277-295

Introduction

Agung, Bromo, and Sinabung are active volcanoes located in the Sunda Arc which have a high volcanic activities over the last decade. These three active volcanoes were chosen as representatives of the Sunda Arc segmentation consisting of the Sumatra and Java Arc Zones which have different plate movement speeds with different eruption characteristics (Figure 1). Since

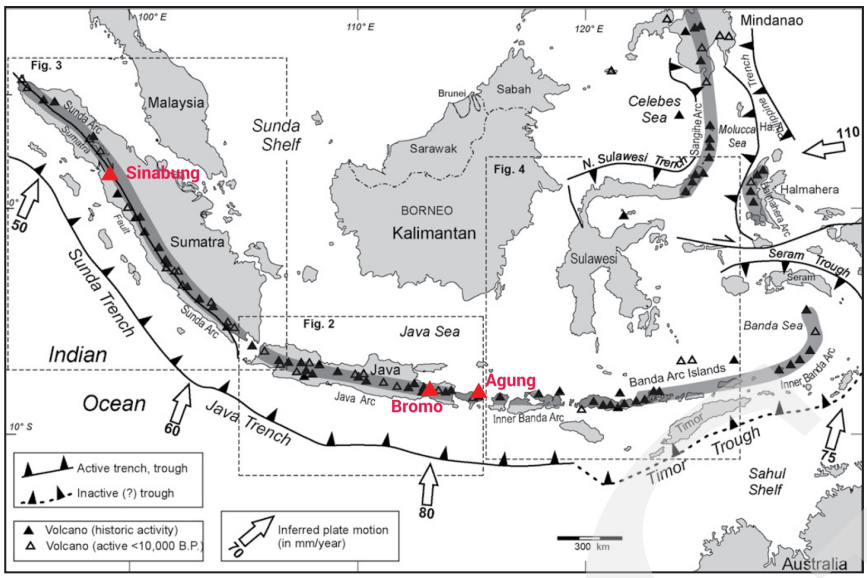

Figure 1. Sinabung, Bromo, and Agung Volcanoes lies in Sunda Arc with different velocity of plate movement (Hochstein and Sudarman, 2008).

Indonesia's volcanoes are dominantly located in subduction zones, their SO_2 gas emissions were considered as the largest part of the total global SO_2 emissions (Textor *et al*., 2004).

SO_2 is one of magmatic gases that has an important role in volcanic activity (Shinohara, 2013). SO_2 emission can provide information about the magnitude of the eruptions, or the mechanism of gas released from a volcano at a certain time (Granados *et al*., 2001), and can provide information of pressure or the source depth (Burton *et al*., 2007). In addition, the composition of volcanic gases is very useful for understanding the character of a volcano (Aiuppa *et al*., 2007), besides it can predict when the eruption will occur (Glasow, 2008).

Similar with volcanic gases, thermal manifestations around the centre of volcanic activity can be an important indication of the increasing volcanic activity (Coppola *et al*., 2015). Detected thermal from the centre of the volcanic activity can be associated with the release of volcanic gases, heated surfaces due to convection from hydrothermal activity, induction of magma ascent to shallower depths, or heat radiation from lava flows on the surface (Harris, 2013). Therefore, monitoring the surface temperature around the centre of volcanic activity is mostly to identify the precursor of the increasing volcanic activity and to understand the volcanic system (Harris and Stevenson, 1997).

The measurement of surface temperature and SO_2 emission rate methods has a very fast development, starting from direct (in-situ) sampling to remote sensing methods. A direct sampling of volcanic gas carried out for analyzing in a laboratory is the most accurate method until nowadays, because it can minimize contact between volcanic gas samples and ambient air, so that gas dissolution can be neglected (Giggenbach, 1975). However, direct measurement of volcanic gases cannot always be carried out because the sampling location access is difficult or the volcanic activity increases, causing the risk of sampling becomes too high. Therefore, the development of temperature and volcanic gas measurements using remote sensing methods based on space-based and ground-based measurement data is very potential in monitoring volcanic activity, because it can provide long-term data set and safe even when volcanoes are in a crisis phase (Rivera, 2011; Carn *et al*., 2016; and Silvestri *et al*., 2020).

In this study, the SO_2 emission data was integrated from DOAS measurement and OMI images with the surface thermal anomaly derived from ASTER TIR images to assess the eruptions over the last decade.

Methods and Materials

Ground-Based Measurement of SO_2 Emission Rate

The SO_2 emission rate measurement used two types of DOAS: mobile DOAS (traverse method) and scanning DOAS. Mobile DOAS in Agung Volcano was used at 10-16 km in the north to the south flank of Agung Crater, whereas in Bromo Volcano, it was used at 2 - 4 km from the crater rim. The measurement method used an Ocean Optic S2000 (Ocean Optic Inc.) spectrometer with spectral radiance and resolution between 280 - 420 nm and 0.6 nm, respectively. The on-board spectrometer, a moving vehicle beneath the plume, was connected to GPS and telescope to record the measurement track positions, and to measure the trajectory distance from the plume source, respectively (Kantzas *et al*., 2010; Kern *et al*., 2020). On the other hand, scanning DOAS were installed permanently in three different stations at 5 - 7 km on the east and southeast sides of Sinabung Volcano. Scanning DOAS used an Ocean Optic USB2000 spectrometer with the scan angle of 3 - 4°, spectral range of 245-385 nm, and spectral resolution of 1.1 nm to measure the SO_2 emission rate automatically during the typical west-wind direction.

The DOAS method used the absorption characteristic of SO_2 gas molecules along a path of known length in the atmosphere. The method applied the Beer-Lambert law by considering Rayleigh and Mie Scattering as follows:

$$\tau'(\lambda) = ln\left(\frac{I_o'(\lambda)}{I(\lambda)}\right) = \int_o^L \left(\sum_i \sigma'_i(\lambda)\, x\, ci\,(l)\right) dl \quad \text{..... (1)}$$

where:
$\tau'(\lambda)$ is differential optical density,
$I_o'(\lambda)$ is derived from the measured spectrum by applying a low-pass filter or interpolating across the tops of narrow-band structure in the spectrum,
$I(\lambda)$ is a measured spectrum,
L is total light path length,
$\sigma'_i(\lambda)$ is the differential absorption cross-section,
$c_i(l)$ is the concentration of the absorber i (Kern, 2009).

Passive DOAS measurements used scattered sunlight as the light source. Then, the differential optical density was retrieved by using a solar spectrum outside the atmosphere as the Fraunhofer reference, applied to satellite measurements. However, for ground-based measurement, Fraunhofer reference spectrum was measured by the instrument by looking in a direction which the absorber of interest is in lower abundance (Kern, 2009). In this case, the reference was measured by looking away from the plume.

The DOAS method measures the SO_2 column density S rather than concentration as follows:

$$S = \int_o^L ci\,(l)\, dl = \frac{\tau'(\lambda)}{\sigma'(\lambda)} \quad \text{..... (2)}$$

where:
S is SO_2 column density,
L is total light path length,
$c_i(l)$ is a concentration of the absorber i,
$\tau'(\lambda)$ is differential optical density,
$\sigma'_i(\lambda)$ is differential absorption cross-section (Kern, 2009).

All the spectra were corrected by dark current and electronic offset. The reference spectra included in the nonlinear fit were obtained by convolving high resolution SO_2 (Bogumil *et al*., 2003) and O_3 (Voigt *et al*., 2001) cross-sections with the instrument line shape. The Fraunhofer reference spectrum and ring spectrum were calculated in DOASIS software integrated with mDOAS software. Following the fitting reference spectrum process, the SO_2 emission rate was calculated from retrieved SO_2 column densities (S) as follow:

$$\bar{\epsilon}_{SO_2} = S\, x\, D\, x\, Vw\, x\, cos\left(T_\alpha - W_\alpha + \frac{3\pi}{2}\right) \quad \text{..... (3)}$$

where:
$\bar{\epsilon}_{SO_2}$ is emission rate,
S is SO_2 column densities,
D is distance,
Vw is wind speed,
T_α is travel angle,
W_α is wind angle (Optical Sensing, 2007).

The wind speed was obtained from the National Oceanic and Atmospheric Administration Global Forecast System (NOAA GFS) of wind model re-analysis data reports.

Space-Based Measurement of SO_2 Emission Rate

SO_2 emission from Agung, Bromo, and Sinabung Volcanoes assessed by the Ozone Monitoring Instrument (OMI) is an ultraviolet/visible (UV/VIS) spectrometer launched on July 2004 by NASA Earth Observing System (EOS) Aura satellite. OMI pixel size is 13×24 km^2 at nadir (along x across-track). OMI spectral ranges between 270 and 500 nm in the UV/VIS region, using two channels with spectral resolution of about 0.5 nm. UV channel varies from 270 to 365 nm and VIS channel ranges between 365 - 500 nm. There are two subchannels of UV with the range of 270 - 310 nm for UVI-1 and 310 - 365nm for UV-2. OMI data in this study was available online (https://so2.gsfc.nasa.gov/index.html). Principal component analysis (PCA) has been applied to re-analyze the OMI dataset with the latest retrieval algorithm (Carn *et al*., 2017). The standard deviation of PCA retrieved background SO_2 ~0.5 Dobson units (DU), where 1 DU= 2.69×10^{26} molecule km^{-2} (Carn *et al*., 2017).

Land Surface Temperature Measurement

The surface temperatures of Agung, Bromo, and Sinabung Craters were derived from ASTER TIR in a spectral range between 8.125-11.65 µm. The ASTER TIR images in level 1T Precision Terrain Corrected Registered At-Sensor Radiance (AST_L1T) were processed to obtain surface temperature in period of 2010-2020 (Table 1). The ASTER TIR data were retrieved from the NASA Earth Data centre (https://search.earthdata.nasa.gov/search). The night-time acquisition data were selected to obtain a high signal-to-noise ratio and to decrease the solar heating effects (Reath *et al*., 2019).

ASTER TIR images were inspected visually for cloud cover of less than 10% over the three volcanoes, corrected radiometrically and atmospherically. The thermal emissivity separation (TES) method was used to calculate the surface temperature by excluding the surface emissivity (Abrams, 2000; Reath *et al*., 2019).

Following Boori *et al*. (2015), the ASTER TIR was calibrated by converting each image pixel to radiance as follows:

$$L_\lambda = (DN\text{-}1) \times UCC \quad \text{..... (4)}$$

where:
L_λ refer to spectral radiance,
DN is digital number,
UCC are the published Unit Conversion Coefficients for each ASTER TIR channel (Table 2).

After converting the *DN* to radiance, the thermal atmospheric correction was performed to remove the atmospheric contributions. Assuming reflection and scattering of solar radiation are

Table 1. ASTER TIR L1T Data Collection for Ten Year Observation of Agung, Bromo, and after Converting the DN to Radiance. Thermal Atmospheric Correction was Performed by Sinabung Volcanoes

Year	Number of ASTER Images			Acquisition
	Agung Volcano	Bromo Volcano	Sinabung Volcano	
2010	9	8	2	Night-time
2011	10	21	1	Night-time
2012	7	14	1	Night-time
2013	6	12	0	Night-time
2014	7	10	2	Night-time
2015	8	2	0	Night-time
2016	10	4	3	Night-time
2017	3	5	3	Night-time
2018	9	0	3	Night-time
2019	10	9	4	Night-time
2020	9	5	3	Night-time

Table 2. ASTER Radiance Scale Factors

Band	UCC
Band 10	0.0068
Band 11	0.00678
Band 12	0.00659
Band 13	0.00569
Band 14	0.00522

ignored, the radiation from the surface received by the sensor will be reduced by the atmosphere transmission as follows:

$$L(\lambda, T_s) = \frac{[L(\lambda, T^*) - L_u(\lambda)]}{[\tau(\lambda)\,\varepsilon(\lambda)]} \quad \text{..... (5)}$$

where:
$L(\lambda, T_s)$ is radiance of targeted surface,
$L(\lambda, T^*)$ is radiation obtained from the sensor,
$L_u(\lambda)$ is atmospheric upwelling radiance,
$\tau(\lambda)$ is transmission, and $\varepsilon(\lambda)$ is emissivity.

The radiation emitted from the surface in the range of thermal infrared wavelength represents their kinetic temperature and emissivity (Saepuloh *et al.*, 2020) related to physical properties of the surface. In this study, the emissivity normalization technique has been used to calculate the temperature for every pixel by taking an assumption that surface emissivity is homogeneous. Then, the brightness temperature was calculated as follows:

$$T_{\lambda,i} = \left(\frac{I_{\lambda,i} - L_u(\lambda) - (1 - \varepsilon_r)\, Ld(\lambda)\tau_\lambda}{\varepsilon_r \tau_\lambda} \right) \text{..... (6)}$$

where:
ε_r defined as reference emissivity,
$I_{\lambda,i}$ is radiance measured in band λ for pixel i,
$Ld(\lambda)$ is downward radiance,
τ_λ is atmospheric transmissivity for λ band (Rolim *et al*., 2016).

In this study, brightness temperature was retrieved from TIR bands (8.125 μm - 11.65 μm).

All the remote sensing data derived from satellites and field measurements were verified with the seismic data as the real time measurement from each volcano.

Result and Analysis

Agung Volcano

In Agung case, the increasing surface temperature around the crater showed the first sign of the unrest phase of this volcano on November 15th, 2022. Thermal data analysis of Agung Volcano was performed in the period of 2010-2020 and the main eruptive events in the period of 2017-2019 (Figure 2). ASTER night observations well defined the increasing surface temperature at Agung Crater area since they had low thermal inertia (Figure 3). In the volcanic rest period (2010-2016), the mean of surface temperature is about 18°C. This value is defined as a background temperature in this analysis. Based on quartile analysis, the surface temperature was classified into four main quartiles. The lower quartile (Q1) is 17°C, the median (Q2) is 19°C, and upper quartile (Q3) is 25°C, whilst the highest quartile (Q4) is 114°C. The background temperature lies in Q2, and the thermal anomaly was interpreted to lie in Q3 and Q4 (Figure 4).

The surface temperature of Agung Crater on September 12th, 2017 - November 15th, 2017, increased up to 25° - 30°C. The increased surface temperatures were not followed by the increasing of SO_2 emission rate in this period. The SO_2 emission rate was detected by DOAS measurement after the first eruption on November 21st, 2017, and SO_2 emission rate was obtained to be 936 ± 155 tons/day. The SO_2 emission rate increased significantly after the second eruption on November 25th, 2017, about 5422 ± 876 tons/day, and it was recorded as the highest emission (Figure 4).

The limitation of the optical sensor against the cloud cover made it difficult to verify the increased pre-eruptive thermal activity on January 2019 to March 2019. But on April 27th, 2019, the surface temperature increased up to 42°C, three days prior to the eruption on April 30th, 2019. The high thermal anomaly was detected on May 13th,

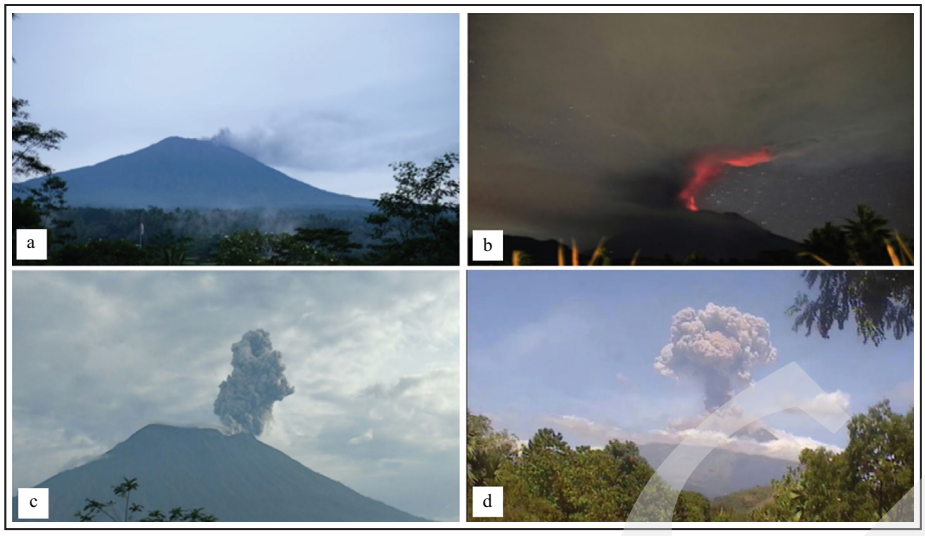

Figure 2. Agung Volcano eruptions photographs of (a) First eruption occurred on November 21, 2017 (photo credit: Martanto, 2017); (b) Second eruption occurred on November 25, 2017 (photo credit: Martanto, 2017); (c) Eruption on January 15, 2018 (photo credit: Magma Indonesia); (d) Eruption on May 31st, 2019 (photo credit: Magma Indonesia).

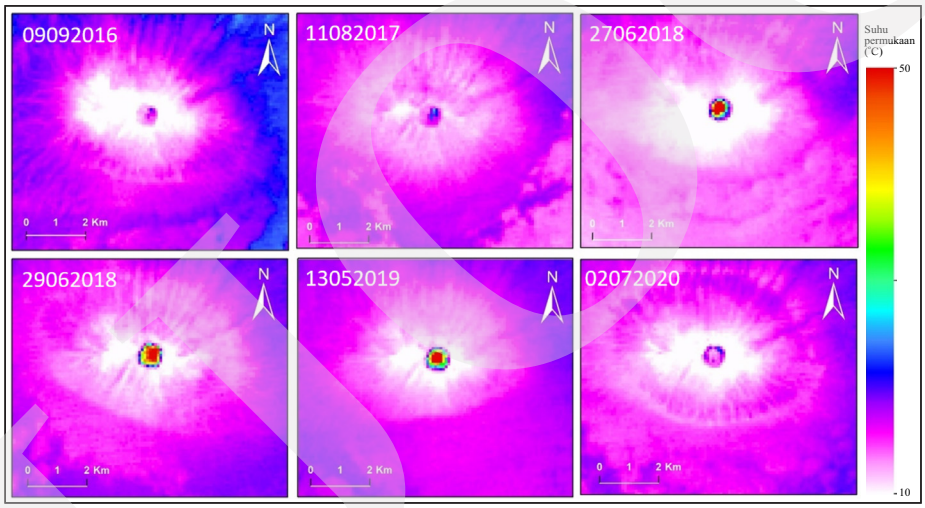

Figure 3. ASTER TIR images in the night-time acquisition detected thermal radiations at the summit of Agung Volcano presented by bright tonal in the middle termed as hotspot prior- and syn-eruption periods.

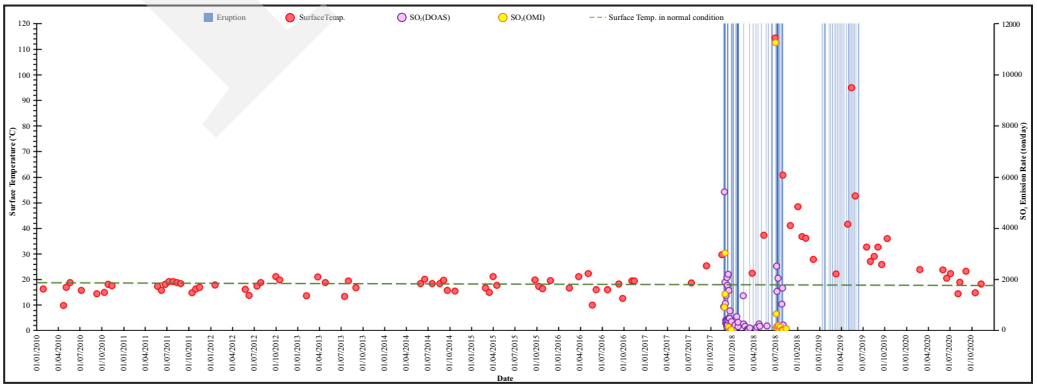

Figure 4. Correlation between SO_2 emission rate and surface temperature of Agung crater compared to eruption event during 2010 - 2020 period.

2019, and the surface temperature was up to 95°C. Detection thermal anomaly was not followed by the increase SO_2 emission rate. The eruption was continuing from May until June 13th, 2019, and the surface temperature tended to decrease. Eruptive phase terminated in 2019, and in 2020 Agung Volcano entered its relaxing phase.

Since the ground-based measurements were not performed continuously, the observation of SO_2 emission from OMI image was used to fill the data gap. OMI image successfully recorded a big eruption of Agung Volcano. From OMI data, it was observed that this volcano had a strong SO_2 emission in the period of November 26th -November 29th, 2017 (992-3,035 tons/day), and the highest SO_2 emission occurred on June 29th - July 2, 2018 (661-11,249 tons/day). The OMI result has a strong correlation with thermal anomalies detection. After August 24th, 2018, the SO_2 emission from Agung Volcano was not detected by OMI images.

Bromo Volcano

In contrast with Agung Volcano that emitted SO_2 gas only in its eruptive periods, Bromo Volcano has persistent strong passive and active degassing. In periods of 2010-2020, Bromo Volcano has three eruption periods: 2010, 2016, and 2019 (Figure 5). In this study, SO_2 emission rate measurement using mobile DOAS with traverse method was performed at the radius of 1-5 km on April 7th - 14th, 2019, and the SO_2 emission rate between 196 - 325 tons/day. Besides using mobile DOAS, SO_2 emission rate in the period of July - November 2016 was measured using portable scanning DOAS which was 131-440 tons/day. In addition, Bani (2013) performed DOAS measurement with traverse method, and the SO_2 emission rate was 27 tons/day. Aiuppa *et al*. (2015) obtained SO_2 emission rate of Bromo Volcano was up to 168 tons/day using UV Camera. All the measurements were performed on a passive degassing of Bromo Volcano (Figure 6).

Since Bromo Volcano had lack of gas measurement, OMI image complemented the SO_2 emission data of Bromo Volcano. The results of processing OMI image data were obtained from the Global Sulfur Dioxide Monitoring page of the Atmospheric Chemistry and Dynamic Laboratory

Figure 5. Photographs of Bromo eruptions showing an active degassing in (a) 2010 (Zaennudin, 2011), (b) 2016 (photo credit: Aan Subhan, 2016) , (c) 2019 (photo credit: Magma Indonesia), and (d) a passive degassing in 2020 (photo credit: Magma Indonesia) presented by magmatic material and steam ejections, respectively.

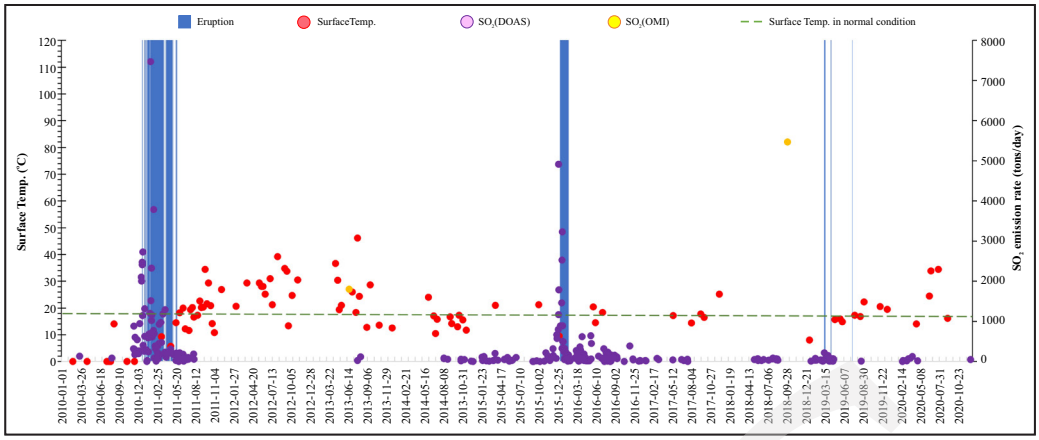

Figure 6. Eruption events of Bromo Volcano presented by blue bars overlaid on temporal SO_2 emission rate and surface temperature derived from OMI, DOAS, and ASTER TIR images.

(https://so2.gsfc.nasa.gov/). The SO_2 mass of Bromo Volcano based on OMI images were distinguished between passive and active degassing. The average of SO_2 mass in the passive degassing phase was 174 tons. Prior to the eruption on December 23rd, 2010, the SO_2 mass that was emitted from Bromo Volcano increased significantly up to 948 tons since December 12th, 2010 (two weeks before the eruption). On December 19th to December 21st, 2010, the SO_2 mass increased up to 2,105 tons and 2,001 tons, respectively. While in the eruption phase, the highest SO_2 emission (active degassing) was up to 7,472 tons (Figure 6).

Similar to the 2010 eruption, the SO_2 mass of Bromo Volcano was observed significantly increase on December 24th, 2015, up to 665 tons (two weeks prior the eruption on January 8th, 2016). The highest SO_2 emission was 4,918 tons on January 2nd, 2016, as the Bromo eruptive phase (Figure 6).

The surface temperature of Bromo Crater was analyzed based on ASTER TIR images at the night time acquisition in the period of 2010 - 2020 (Figure 7). During its rest period (separating thermal data when there is no eruption), the average surface temperature of Bromo Crater was 18°C. This value was set as the background temperature. Based on the quartile analysis, the data set for the surface temperature of Bromo Crater in the last decade was classified into four quartiles. The lower quartile (Q1) value was14°C, the middle quartile (median) was 18°C, the upper quartile (Q3) was 24°C, and the maximum value (Q4) of surface temperature data was 46°C. Based on the quartile analysis, the background temperature of Bromo Crater was in Q2, and the thermal anomaly is interpreted to be in Q3 to Q4.

The surface temperature of Bromo Volcano did not show a significant increment in the eruption phase, especially in the 2010 eruption. However, during the repose phase, the surface temperature of this volcano increased several times and interpreted as a thermal anomaly. Compared with SO_2 emission rate, there was a tendency that thermal anomaly at Bromo Volcano was detected when SO_2 emission were not detected.

Sinabung Volcano

Sinabung Volcano had five eruption periods within 2010 - 2020. The first eruption occurred in 2010, the second eruption in 2013, the continuous eruption lasted in 2015 - 2018, followed by the eruption that occurred in 2019, and the last one was the eruption in 2020 (Figure 8).

The first eruption occurred when Sinabung volcanic activity was unmonitored. OMI images helped to see SO_2 emission from this volcano. The SO_2 mass of Sinabung Volcano was 127 tons on August 28th, 2010, based on OMI image. It recorded one day after the first eruption of the volcano from the satellite. On the other hand, ground based measurement of SO_2 emission from Sinabung Volcano was performed on September 4th, - September 23rd, 2010, and the measured SO_2 was 259 - 972 tons/day (Gunawan *et al.*, 2019).

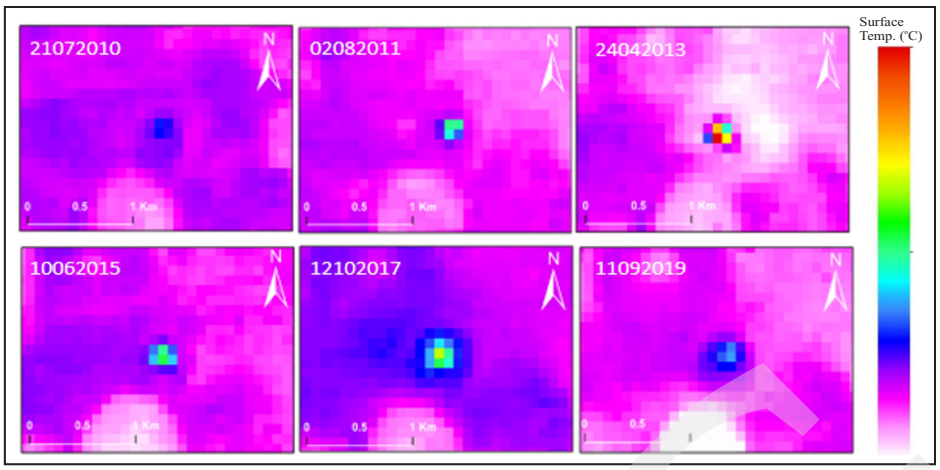

Figure 7. ASTER TIR images in the night-time acquisition detected thermal radiations at the summit of Bromo Volcano presented by bright tonal in the middle termed as hotspot prior- and syn-eruption periods.

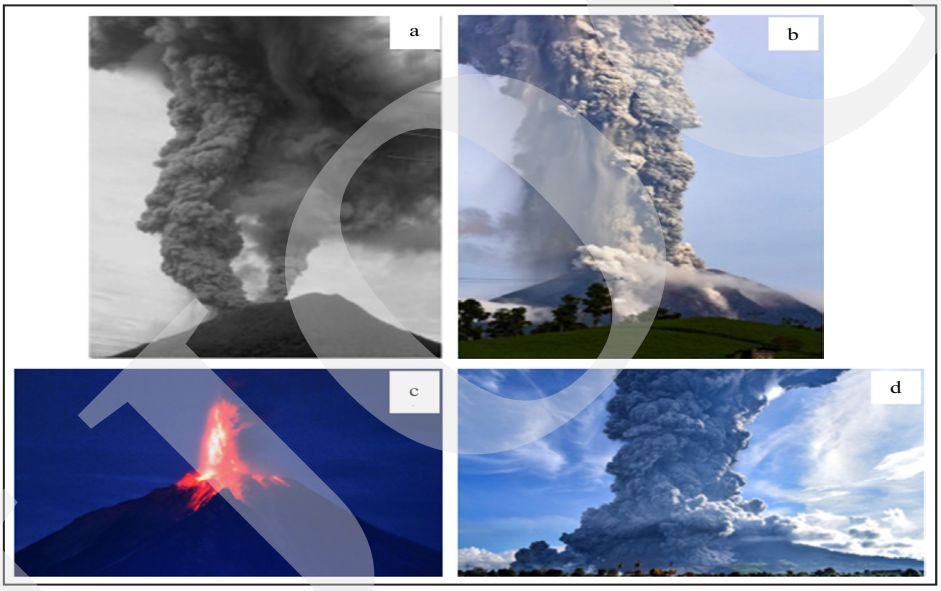

Figure 8. Photographs of Sinabung eruptions in (A) 2010 (Gunawan *et al*., 2019), (B) 2013 (Gunawan *et al*., 2019), (C) 2017 (photo credit: M.N Ashrori, 2017), and (D) 2018 presented by magmatic material ejections (photo credit: Magma Indonesia).

Furthermore, SO_2 emission from Sinabung Volcano was detected in the 2013 eruption period. The mass of SO_2 emitted by this volcano was in the range of 14 - 26,282 tons on November 8th, 2013 - February 16th, 2014. The mass of SO_2 in this eruption phase was detected to be very high. When the eruption began to decrease, during the relaxation phase for the period of February 18th, 2014 - March 7th, 2015, the SO_2 mass recorded by OMI image data was in the range of 11 - 1,283 tons. Meanwhile, the measurement of SO_2 emission rate using the portable scanning DOAS was carried out before the 2013 eruption events, in the period of September 16th - November 18th, 2013, and the SO_2 emission rate fluctuated between 121 - 814 tons/day (Figure 9).

For the SO_2 emission rate considered as the valuable data, since August 20th, 2016, three permanent DOAS stations as part of Network for Observation of Volcanic and Atmospheric Change (NOVAC) instrument was installed in Sinabung. The obtained data from scanning DOAS was re-analyzed and re-filtered for more than 80% plume completeness. The ground based SO_2 emission

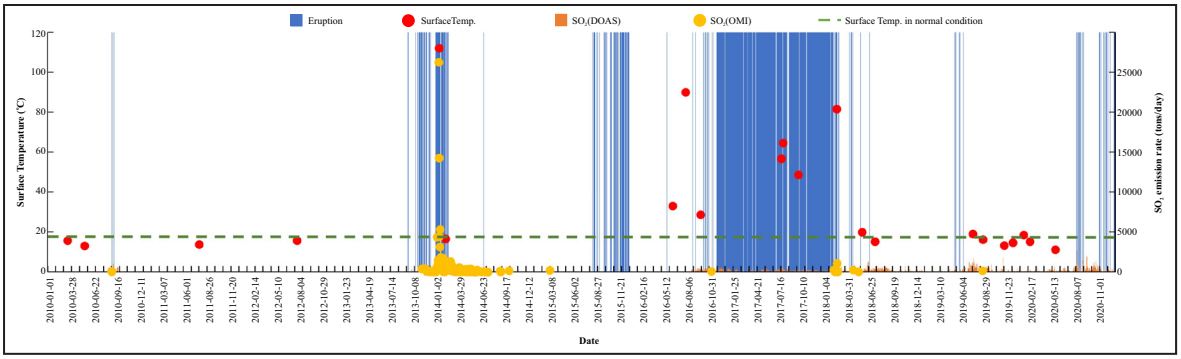

Figure 9. Eruption events of Sinabung Volcano presented by blue bars overlaid on temporal SO_2 emission rate and surface temperature derived from OMI, DOAS, and ASTER TIR images.

rate data was fluctuating before the big eruption, SO_2 emission rate data tended to decrease and became higher when the eruption occurred.

Thermal data of Sinabung Volcano was analyzed in the period of 2010 - 2020, and the observation of ASTER TIR images at the night-time acquisition showed the increment pattern of the surface temperature around this crater. The surface temperatures before the first eruption of Sinabung Volcano were recorded on March 2010 and May 20th, 2010, about 16°C and 13°C, respectively. Some data were not well recorded since ASTER recycle time was sixteen days and due to cloud cover around the Sinabung Volcano. But overall, ASTER TIR images successfully captured the increase of surface temperature which were detected as anomaly thermal that had a strong correlation with eruption events. Besides that, ASTER TIR images also detected the changes of lava flow and Pyroclastic Density Currents (PDC) direction in Sinabung (Figure 10).

Discussion

Agung Volcano

Based on the measurement of SO_2 emission rate, both from the field and satellite images, combined with thermal anomaly analysis that compared to Agung seismicity in the period of 2010-2020 (Figure 11), Agung volcanic activity was divided into four phases as follows:

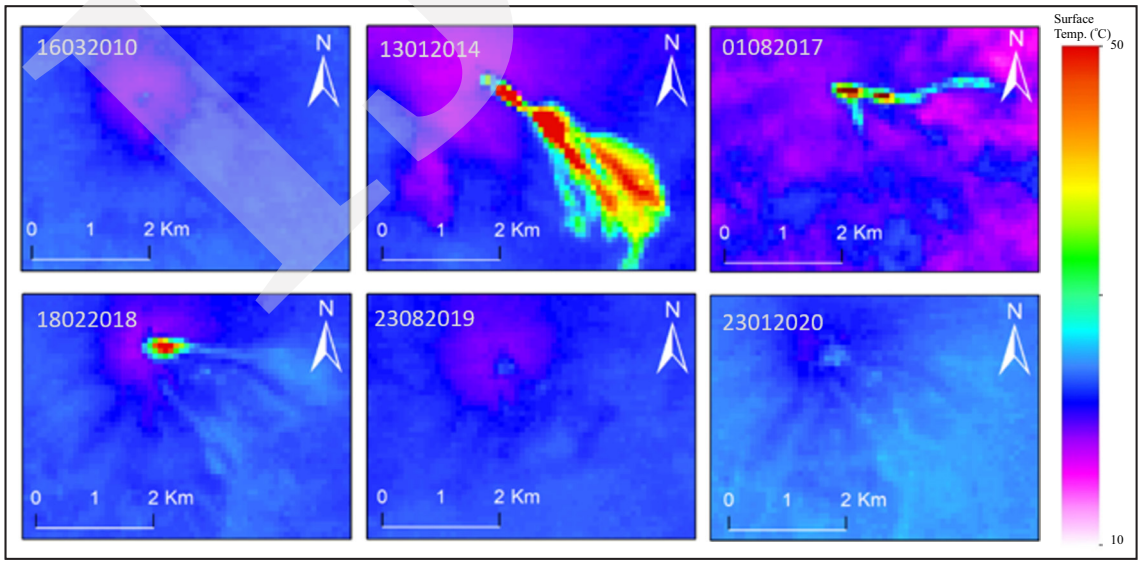

Figure 10. ASTER TIR images in the night-time acquisition detected thermal radiations at the summit of Sinabung Volcano presented by bright tonal in the middle termed as hotspot prior- and syn-eruption periods.

1. Repose phase (January 1st, 2010 - September 14th, 2017).
   The background temperature was 18°C and the maximum temperature was 22°C. The seismicity was dominated by tectonic earthquakes, and the SO_2 emission was not detected. This condition related to magmatic state, no magma movement. So, the SO_2 was not emitted to the surface.
2. Dyke formation phase (September 15th - November 20th, 2017.
   This phase was marked by the increase of Deep Volcano-Tectonics (Deep VT) since August 18th, 2017, followed by Shallow Volcano-Tectonics (Shallow VT) since September 20th, 2017, with thermal anomaly detected. These signs were interpreted that the magma was moving into the shallow depth but did not reach the surface (Syahbana *et al.*, 2019). InSAR results during September-October showed the formation of a dike at ~10 km depth between Agung and Batur (Albino *et al*., 2019; Syahbana *et al*., 2019). The result of the DOAS measurement from October 1st - November 14th, 2017 showed that the SO_2 was still not detected. It is assumed that in this phase, the magmatic volatile was being scrubbed by the hydrologic system beneath the Agung Crater. Direct injection of magmatic gases into meteoric water produced acidic hydrothermal fluids. Magmatic gases were scrubbed involving disproportionation reaction:

$$4SO_{2(g)} + 4H_2O_{(aq)} \rightleftharpoons H_2S_{(aq)} + 3H_2SO_{4(aq)} \quad \text{..... (7)}$$

$$3SO_{2(g)} + 2H_2O_{(aq)} \rightleftharpoons S_{(s,l)} + 2H_2SO_{4(aq)} \quad \text{..... (8)}$$

Cooling temperature below 400°C will make the equilibrium shifted to the right (Symonds *et al*., 2001).

3. Vent clearing and drying-out the conduit (November 21st to 22nd, 2017).
   The third phase was marked by the eruption of Agung Volcano on November 1st, 2017. This eruption cleared the vent and created an outgassing pathway, the high SO_2 emission rate was detected on November 22nd, 2017. The presence of SO_2 in the volcanic gas indicated that magma migrated to the shallower depth and the magmatic gases penetrated the hydrologic system without being scrubbed by the groundwater. The presence of SO_2 might be due to the lack of groundwater in the shallow hydrologic system beneath the crater. This condition allowed the SO_2 to be released into the atmosphere. In this phase, it is assumed that the shallow hydrologic system beneath Agung Crater was drying out when the magma was moving towards the surface allowing SO_2 gas to pass through the system. This is a step toward magmatic activity.
4. Magmatic activity (November 25th, 2017-June 15th, 2020).

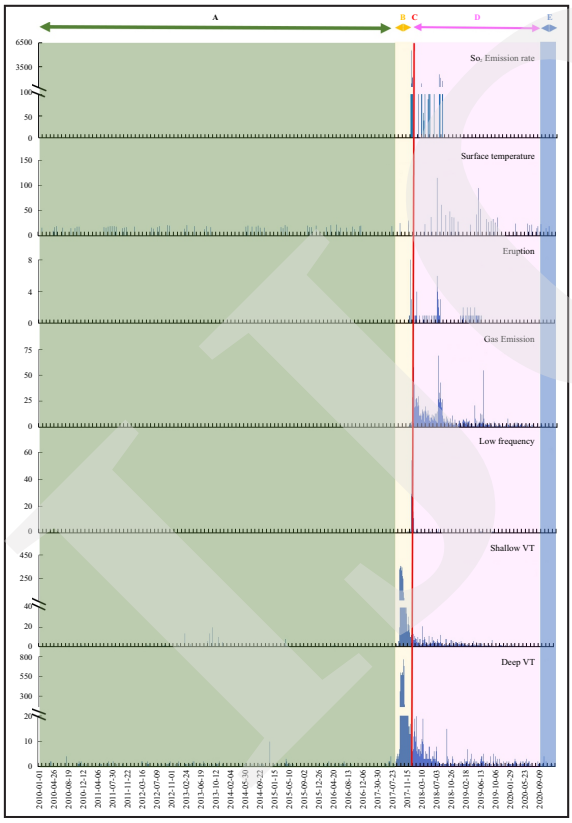

Figure 11. Agung volcanic activity in the period 2011 - 2020 is divided into four main phases. (a) Repose period of Agung Volcano, (b) Unrest phase is indicated by the swarm of Deep VT and followed by Shallow VT. This correlated with the formation of dyke (c) Magma is already near the surface opening pathway process, and the conduit is drying out. So, the SO_2 can be emitted from Agung Volcano. (d) Magmatic phase released volcanic material, such as lava and pyroclastic fall. (e) Relaxation phase was defined as a low magma supply in Agung Volcano tended to be back to repose phase.

In this phase, ASTER TIR night-time images showed the strong correlation of thermal anomaly result corresponded with the ejecting of volcanic material, such as lava and pyroclastic fall. A day after the beginning of the continuous magmatic eruption event, high SO_2 emission rate was detected. In the period of August 2018 until June 2019, even there was no explosive eruption, but strong thermal anomalies were detected. These data were interpreted to associate with effusive eruption followed by another explosive eruption on February - June 2019.

After June 15th, 2020, the seismicity of Agung Volcano tended to decrease, anomaly thermal and SO_2 emission were not detected. This relaxation phase reflected a low magma supply, and hydrothermal system might be re-established. The hydrothermal system might cause the magmatic gas like SO_2 be scrubbed and not be released to the surface. The four different eruption phases were illustrated in Figure 12.

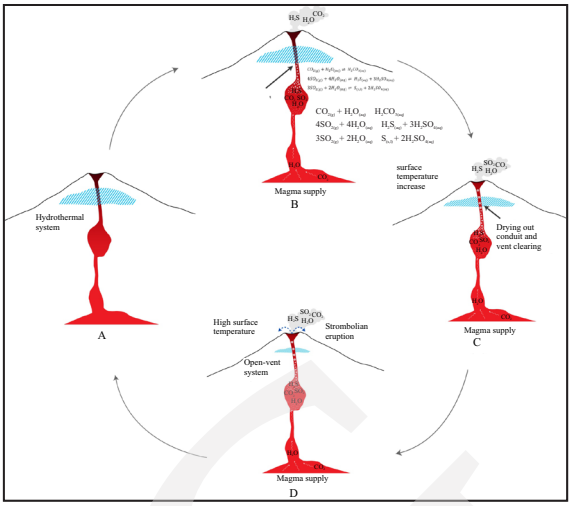

Figure 12. Illustration of magmatic plumbing system at Agung Volcano (Syahbana *et al*., 2019) during period of 2010 - 2020 based on seismicity, SO_2 emissions, and surface temperature: (a) repose period; (b) initial ascending magma; (c) interaction the heat transfer of magma ascent with hydrothermal system; (d) opening conduit prosecuted by the strombolian eruption.

Bromo Volcano

Bromo Volcano has three eruptive periods in 2010-2020, which are in 2010, 2015-2016, and in 2019. Based on Bromo seismicity, there are different patterns from three eruptions (Figure 13). In 2010, the increase of Bromo volcanic activity started with the significant increase of shallow volcanic earthquake. This phase was interpreted as magma movement from the shallow depth to the near surface. The increase of SO_2 emission which were detected approximately two weeks before the eruption indicated that the magma was close to the surface and strong degassing occurred, because the volatiles exsolved from magma due to loss of pressure. The magma ascent usually followed by thermal anomaly, but in this case, no significant thermal anomaly was observed from the surface of Bromo Crater. These phenomena were estimated because Bromo Volcano has an open system, so there is a continuous release of thermal energy.

The eruption of Bromo Volcano in 2015 was preceded by the increase of volcanic tremor amplitude. However, SO_2 emission was detected two weeks before the eruption, but it was not high. This phenomenon was interpreted that the magma supply in 2015 eruption was not as high as in 2010. In 2019, Bromo eruption occurred without any clear precursor, neither from seismicity nor SO_2 emission. The type were estimated as the phreatic type, so water vapour was dominated by the volcanic gas. These could reflect the lower magma supply compared to the eruption in 2015-2016.

Since the thermal anomaly has no strong correlation with seismic signal and SO_2 emission rate, Bromo volcanic activity was divided based on the seismic signal and the fluctuation of SO_2 emission rate into three main phases, which were repose phase, passive degassing phase, and eruptive phase (Figure 14).

At the repose phase, Bromo magmatic system was in equilibrium, and there was no magma supply. In passive degassing phase, there was magma supply that allows passive degassing. Magma ascent caused decompression and increased magma buoyancy. When decompression occurred, the volatiles were exsolved from magma and allowed nucleation, the growth and expanding of

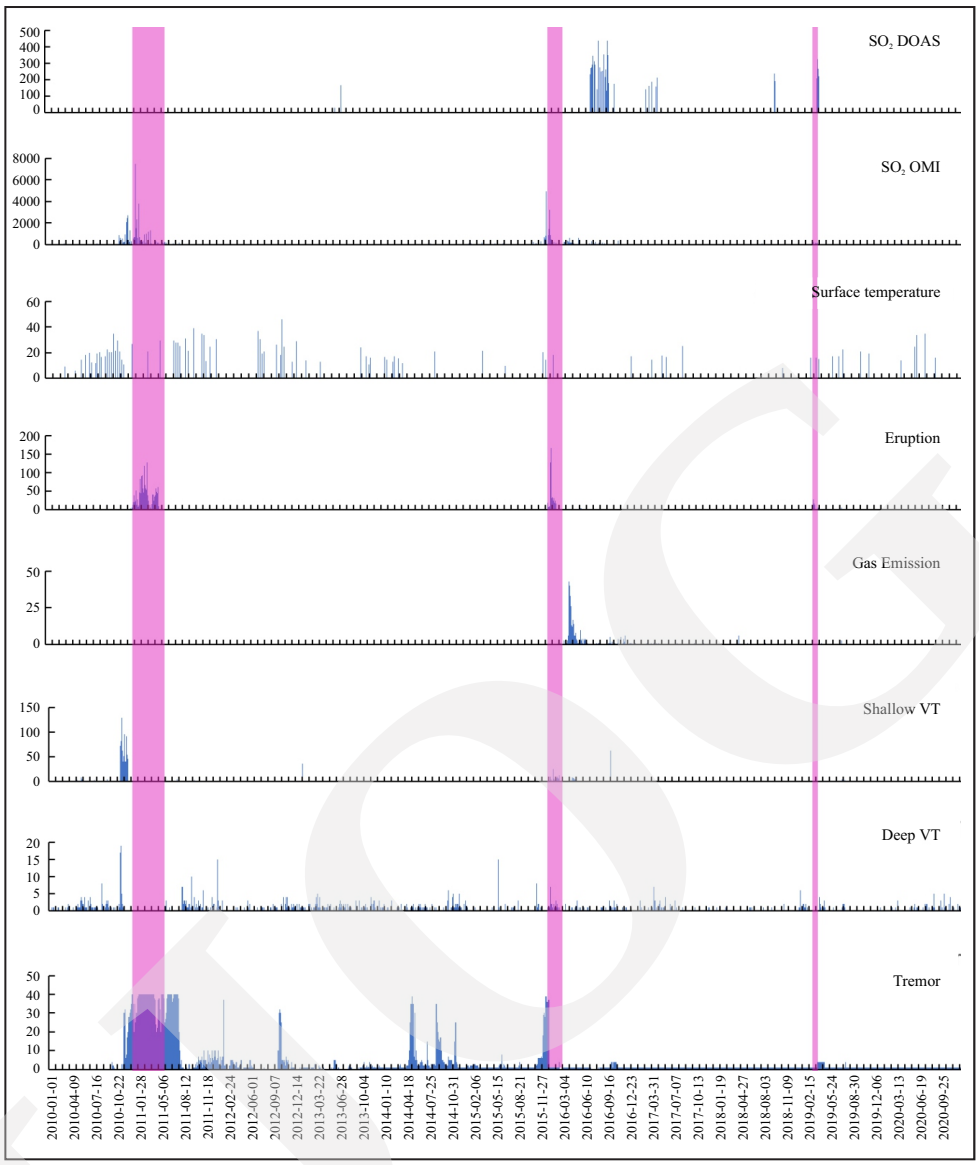

Figure 13. Three eruption periods (pink bars) overlaid on temporal volcanic activities of Bromo Volcano in 2010 - 2020 presented by seismicity statistics. The precursor seismic signatures to the 2010 - 2011 eruptions were identified by the increase of Deep VT and Shallow VT and the significant increment of SO_2 emission rate; the 2015 - 2016 eruptions by the increment both of tremor amplitude and SO_2 emission rate; and 2019 eruptions has the uncleared precursor neither seismicity nor SO_2 emission rate.

bubbles, and coalescence created a pathway for the gas loss (passive degassing). At the eruptive phase, magma ascent triggered decompression, and produced more bubbles that grew, expanded, and caused the overpressure beneath the Bromo Volcano. In general, Bromo eruptions were categorized as phreatic, phreatomagmatic, and strombolian eruptions. After the eruptive phase ended, magma supply tended to decrease, and Bromo Volcano entered a repose phase or passive degassing phase (Figure 14).

Sinabung Volcano

Sinabung Volcano had five eruption periods in 2010 - 2020 (Figure 15). After its long rest period, the precursor of initial unrest phase on August 2010 was identified by 1.4 cm inflated summit (Saepuloh *et al*., 2019). In general, in the last decade, thermal anomaly patterns were detected in the eruptive phase, and SO_2 emission rate correlates with the eruption events of Sinabung Volcano. The first SO_2 emission was recorded by OMI image after the first eruption occurred in

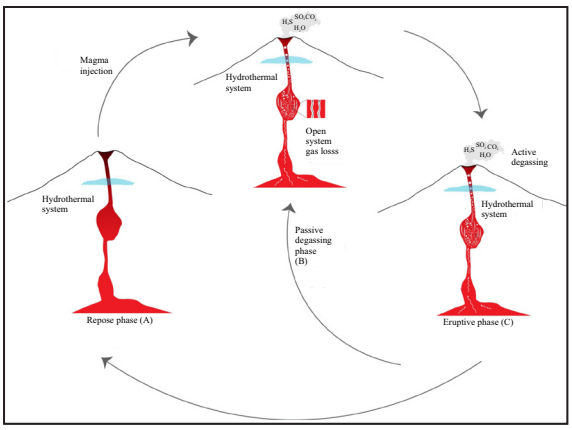

Figure 14. Illustration of magmatic plumbing system at Bromo Volcano during 2010 – 2020 based on seismicity, SO_2 emissions, and surface temperature: (A) repose period; (B) Initial ascending magma; (C) active degassing and explosive eruption. After the eruption phase, Bromo Volcano will be back to passive degassing phase or repose phase.

2010. The eruption destroyed the lava plug, and volcanic gas could be emitted to the atmosphere. The highest SO_2 emission rate was recorded in 2013-2014 eruption indicating that Sinabung volcanic activity had shifted from a phreatic eruption in 2010 to phreatomagmatic 2013, and became the magmatic eruption in 2014 (Gunawan *et al*., 2019). Thermal anomalies from magmatic activity were also successfully recorded by ASTER images showing high surface temperatures from the crater of this volcano.

After the first eruption of Sinabung Volcano in 2010, the seismicity was dominated by deep volcanic earthquakes and shallow volcanic earthquakes that indicated magma movement to the shallow depth. The eruptive periods occurred in a week, but the seismicity showed an intermittent magma supply (Figure 15). Sinabung eruptions in 2013 - 2014 were divided into five main phases. There was phreatomagmatic phase (July - December 18th, 2013), first dome and collapse phase that caused pyroclastic density currents (PDCs) to the south (December 18th, 2013 - January 10th, 2014), lava flow and collapse phase (January 10th - mid-September 2014), second lava dome and collapse phase with PDCs to the south (mid-September 2014 - July 2015), lava dome collapse and ash explosions with PDCs to the southeast and the east (August 2015 - 2018) (Gunawan *et al*., 2019; Kriswati *et al.*, 2020). Nevertheless, the eruptions in 2019 was not preceded by significant increment of seismicity (Figure 15).

Based on the correlation between SO_2 emission rate, thermal anomaly, and seismicity during 2010 - 2020, Sinabung was illustrated to have four main phases. Sinabung has more than four hundred years of repose phase, and in this phase the conduit and magma chamber were in equilibrium condition. Sinabung entered a new eruptive phase in 2010 and has a new injection magma. The ascending magma caused decompression, and magma buoyancy increase. The volatile was exsolved, bubbles grew and expanded, and overpressure occurred triggering explosive eruption. Since the Sinabung Volcano has a viscous magma (Nakada *et al*., 2019; Suparman *et al*., 2021), the lava dome was formed, and degassing occurred. The growth of a lava dome caused destabilization of the dome triggering explosive eruption coinciding with effusive eruption. It can be assumed that one decade data is representative to figure out the cycling of Sinabung volcanic activity. After the explosive and effusive eruption, and the reforming of lava dome, the cycle of explosive and effusive eruption will be repeated, or Sinabung Volcano will enter a repose phase (Figure 16).

In 2019, Sinabung eruption was not preceded by the significant seismicity, and the SO_2 emission rate tended to be low. The SO_2 emission rate was then separated into passive degassing and active degassing. The average of SO_2 emission rate in passive degassing phase was 239 tons/day (Kunrat *et al*., 2021). Based on the correlation between the number of eruption and the SO_2 emission rate in thirty-day interval before eruption, it showed that if SO_2 emission rate was less than 239 tons/day, the number of eruptions was getting bigger. Otherwise, if the SO_2 emission rate was more than 239 tons/day, then the number of eruptions were relatively lower. The number of eruptions were assumed to correlate with the magma ascend rate and the outgassing process beneath (Cassidy *et al*., 2018), and these phenomena were considered to relate with the lava dome forming in Sinabung. When the lava dome grows and there are some

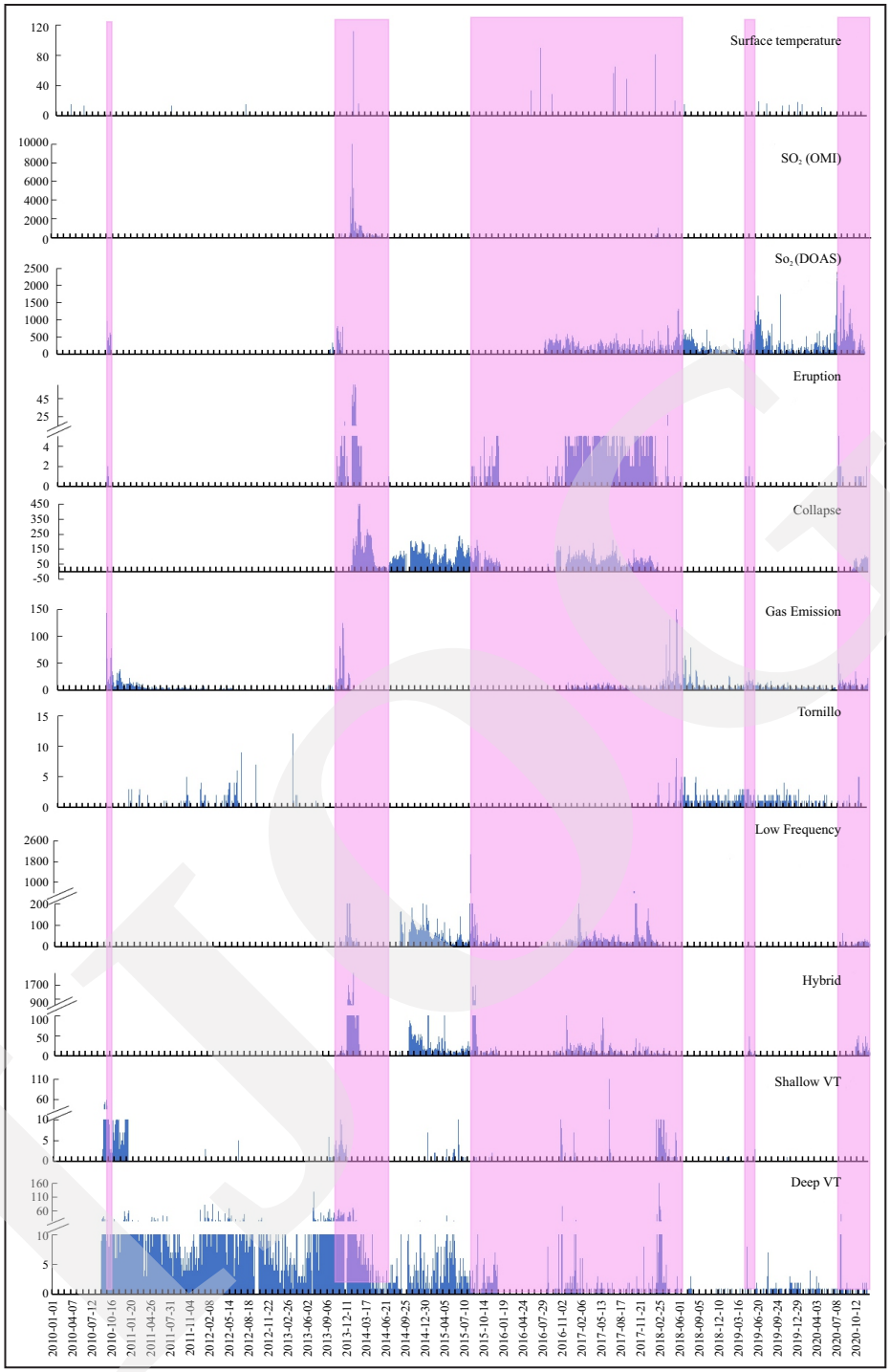

Figure 15. Sinabung volcanic activity in 2010 – 2020. Seismicity dominated by Deep VT and prior the eruption, often followed by Shallow VT in period 2010–2016 that indicates the magma movement to shallow depth. Whereas the 2019 and 2020 eruptions were not preceded by the increment of seismicity.

fractures in the lava dome, volcanic gas can be emitted, so it does not cause a significant overpressure. Meanwhile, if the growth of the lava dome is getting bigger and the fracture in lava dome becomes sealed, then less gas will be emitted, and there will be an accumulation of pressure in the conduit, so it can trigger a bigger eruption. The magnitude of eruptions will depend on the strength of the seal, which determines the accumulated pressure beneath it (Kunrat *et al*., 2022).

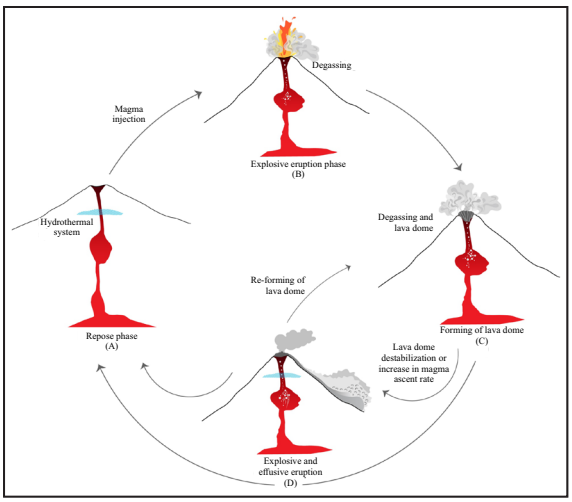

Figure 16. Illustration of magma plumbing system in Sinabung Volcano. (a) Repose phase; (b) The ascending magma triggering explosive eruption; (c) The forming of lava dome; (d) Explosive and effusive eruption phase. After that phase, the re-forming of lava dome occurred, and the cycle of explosive and effusive phase will be repeated, or the Sinabung Volcano entered its repose periods.

Furthermore, the lava dome formed generally characterizes high viscosity of magma. Magma with high viscosity has volatile content distributed in the magma as small bubbles and limiting permeability, so the growth of gas bubbles is not interconnected and prevents the release of gas into the atmosphere (outgassing), then the gas emission rate is relatively low under normal conditions. This causes overpressure in the conduit which triggers an explosive eruption (Cassidy *et al.*, 2018).

Based on SO_2 emission and thermal anomalies of three active volcanoes in this study, Sinabung Volcano has the highest explosivity emitting very high SO_2 gas. It considered to relate with the active continental margin system with granitic crustal thickness of about 50-100 km. So, when magma ascents into the shallow system, it will go through a longer pathway that allows magma differentiation phenomena. In addition, magma has a longer time to allow crystallization to occur that can increase the magma viscosity. The increasing of magma viscosity can inhibit the interconnectedness of magmatic volatile bubbles to form the closed system that increases the potential of explosive eruptions due to overpressure beneath the volcano. Meanwhile, Bromo Volcano that also lies in the active continental margin system, has a thinner crust. Therefore, when the magma rises to the surface, there is less contamination, lower magma viscosity, and gas bubbles can grow and connect to each other to form a degassing pathway (gas loss). The passive degassing process and the regular eruption period in Bromo Volcano reduce the pressure accumulation in the conduit and reduce the potential of large explosive eruptions. Agung Volcano which lies in an island arc system has a much thinner crust, which is about 5-10 km. Thereby, magma pathway that is shorter, has less contamination and lower magma viscosity. However, magma residence time can affect the crystallization process which cause the increase of magma viscosity. The increase in magma viscosity can cause gas bubbles to form a closed system that affect the overpressure in the conduit triggering a large explosive eruption.

Conclusions

Long-term monitoring of SO_2 emission rates and thermal anomaly detection compared to seismicity of each volcano could recognize the onset of the unrest phase volcano, such as in Agung, Bromo, and Sinabung Volcanoes. The long-term data set helped to determine the anomalous signs that required a baseline of volcano background behaviour. The surface temperature background was observed when the volcano was in the rest phase. Additionally, quartile analysis was effective to define the thermal anomaly of the volcanoes.

The SO_2 emission rate in the open vent system was correlated with the magma ascent to the shallow depth. As the open vent system, Bromo Volcano has a persistent strong passive degassing observed from the space base measurement. The magmatic eruption in Bromo Volcano was preceded by the significant increment of SO_2 emission rate. On the other hand, Agung and Sinabung

Volcanoes have closed vent systems, and the SO_2 emission rate was detected after the transition from closed vent to open vent system. However, in closed vent volcanoes such as Sinabung, the decreasing of SO_2 emission must be observed, since it can cause bigger eruption due to pressure accumulation beneath the volcano.

The low thermal anomalies were observed in Bromo Volcano which indicated magma ascent to the shallow depth. The intermittent magma supply in Bromo Volcano was observed from the seismicity data. Since Bromo Volcano was dominated by explosive eruption that occurred in the fast period, the thermal anomalies in eruptive phase were not detected by the satellite image. While in Agung and Sinabung Volcanoes that have explosive and effusive eruption, the thermal anomalies were observed very well.

Combining the remote sensing data from space based and ground based measurement was very potential to provide the comprehensive volcano monitoring data. However, long data set of SO_2 emission rate and land surface temperature based on ground-based measurement are very important to give more insight of volcano dynamic subsurface.

Acknowlwdgement

The authors acknowledge the support from The Centre for Volcanology and Geological Hazard Mitigation (CVGHM) and Volcano Disaster Assistance Programme (VDAP) of the United State Geological Survey (USGS), particularly under the PEER project. The authors extend their sincere gratitude to all the observers of Agung, Bromo, and Sinabung Volcanoes for valuable volcano monitoring data.

References

Abrams, M., 2000. *International Journal of The Advanced Spaceborne Thermal Emission and Reflection Radiometer (ASTER)*: Data products for the high spatial resolution imager on NASA' s Terra platform. *International Journal of Remote Sensing*, p.37-41.

Aiuppa, A., Bani, P., Moussallam, Y., Di Napoli, R., Allard, P., Gunawan, H., Hendrasto, M., and Tamburello, G., 2015. First determination of magma-derived gas emissions from Bromo Volcano, eastern Java (Indonesia). *Journal of Volcanology and Geothermal Research*, 304, p.206-213. DOI: 10.1016/j.jvolgeores.2015.09.008.

Aiuppa, Alessandro, Moretti, R., Federico, C., Giudice, G., Gurrieri, S., Liuzzo, M., Papale, P., Shinohara, H., and Valenza, M., 2007. Forecasting Etna eruptions by real-time observation of volcanic gas composition. *Geology*, 35 (12), p.11-15. DOI: 10.1130/G24149A.1.

Albino, F., Biggs, J., and Syahbana, D.K., 2019. Dyke intrusion between neighbouring arc volcanoes responsible for 2017 pre-eruptive seismic swarm at Agung. *Nature Communications*, 10 (1), 748. DOI: 10.1038/s41467-019-08564-9.

Bani, P., Harris, A.J.L., Shinohara, H., and Donnadieu, F.,2013. Magma dynamics feeding Yasur's explosive activity observed using thermal infrared remote sensing, Geophysical Research Letters, 40 (15), p.3830-3835. DOI: 10.1002/grl.50722

Bogumil, K., Orphal, J., Homann, T., Voigt, S., Spietz, P., Fleischmann, O. C., Vogel, A., Hartmann, M., Kromminga, H., Bovensmann, H., Frerick, J., and Burrows, J.P., 2003. Measurements of molecular absorption spectra with the SCIAMACHY pre-flight model: Instrument characterization and reference data for atmospheric remote-sensing in the 230-2380 nm region, *Journal of Photochemistry and Photobiology A: Chemistry*, 157 (2-5), p.167-184. DOI: 10.1016/S1010-6030(03)00062-5.

Boori, M.S., Vozenilek, V., Balzter, H., and Choudhari, K., 2015. Land Surface Temperature with Land Cover Classes in ASTER and Landsat Data. *Journal of Geophysics and Remote Sensing*, 04 (01), p.2-4. DOI: 10.4172/2169-0049.1000138.

Burton, M., Allard, P., Mure, F., and La Spina, A., 2007. Magmatic gas composition reveals the source depth of slug-driven strombolian explosive activity. *Science*, 317 (5835), p.227-230. DOI: 10.1126/science.1141900.

Carn, S.A., Clarisse, L., and Prata, A.J., 2016. Multi-decadal satellite measurements of global volcanic degassing. *Journal of Volcanology and Geothermal Research*, 311, p.99-134. DOI: 10.1016/j.jvolgeores.2016.01.002.

Carn, S.A., Fioletov, V.E., McLinden, C.A., Li, C., and Krotkov, N.A., 2017. A decade of global volcanic SO_2 emissions measured from space. *Scientific Reports*, 7, 44095. DOI: 10.1038/srep44095.

Cassidy, M., Manga, M., Cashman, K., and Bachmann, O., 2018. Controls on explosive-effusive volcanic eruption styles. *Nature Communications*, 9 (1). DOI: 10.1038/s41467-018-05293-3.

Coppola, D., Macedo, O., Ramos, D., Finizola, A., Delle Donne, D., del Carpio, J., White, R., McCausland, W., Centeno, R., Rivera, M., Apaza, F., Ccallata, B., Chilo, W., Cigolini, C., Laiolo, M., Lazarte, I., Machaca, R., Masias, P., Ortega, M., Puma, N., and Taipe, E. 2015. Magma extrusion during the Ubinas 2013-2014 eruptive crisis based on satellite thermal imaging (MIROVA) and ground-based monitoring. *Journal of Volcanology and Geothermal Research*, 302, p.199-210. DOI: 10.1016/j.jvolgeores.2015.07.005.

Giggenbach, W.F., 1975. A simple method for the collection and analysis of volcanic gas samples. *Bulletin Volcanologique*, 39 (1), p.132-145. DOI: 10.1007/BF02596953.

Glasow, R., 2008. News & views, Nature, 453 *(June)*, p.1195-1196.

Granados, D.H., Gonzales, L.C., Sanchez, N.P., 2001. Sulfur dioxide emissions from Popocatépetl Volcano (Mexico): case study of a high-emission rate, passively degassing erupting volcano. *Journal of Volcanology and Geothermal Research*, 108 (1-4), p.107-120.

Gunawan, H., Surono, Budianto, A., Kristianto, Prambada, O., McCausland, W., Pallister, J., and Iguchi, M., 2019. Overview of the eruptions of Sinabung Volcano, 2010 and 2013-present and details of the 2013 phreato-magmatic phase. *Journal of Volcanology and Geothermal Research*, 382, p.103-119. DOI: 10.1016/j.jvolgeores.2017.08.005.

Harris, A., 2013. *Thermal Remote Sensing of Active Volcanoes*, Cambridge University Press, New York, 758pp.

Harris, A.J.L. and Stevenson, D.S., 1997. Magma budgets and steady-state activity of Vulcano and Stromboli. *Geophysical Research Letters*, 24 (9), p.1043-1046. DOI: 10.1029/97GL00861.

Hochstein, M.P. and Sudarman, S., 2008. History of geothermal exploration in Indonesia from 1970 to 2000. *Geothermics*, 37 (3), p.220-266. DOI: 10.1016/j.geothermics.2008.01.001.

Kantzas, E.P., McGonigle, A.J.S., Tamburello, G., Aiuppa, A., and Bryant, R.G., 2010. Protocols for UV camera volcanic SO_2 measurements. *Journal of Volcanology and Geothermal Research*, 194 (1-3), p.55-60. DOI: 0.1016/j.jvolgeores.2010.05.003.

Kern, C., 2009. *Spectroscopic measurements of volcanic gas emissions in the ultra-violet wavelength region*. University of Heidelberg, Germany, p.1-318. DOI: 10.11588/heidok.00009574.

Kern, C., Lerner, A.H., Elias, T., Nadeau, P.A., Holland, L., Kelly, P.J., Werner, C.A., Clor, L.E., and Cappos, M., 2020. Quantifying gas emissions associated with the 2018 rift eruption of Kīlauea Volcano using ground-based DOAS measurements. *Bulletin of Volcanology*, 82 (7), p.55. DOI: 10.1007/s00445-020-01390-8.

Kriswati, E. and Solikhin, A., 2020. Lava Discharge Rate of Sinabung Volcano Obtained from Modis Hot Spot Data. *Indonesian Journal on Geoscience*, 7 (3), p.241-252. DOI: 10.17014/ijog.7.3.241-252

Kunrat, S., Alfianti, H., Kern, C., Primulyana, S., Lerner, A., and Nurul, M., 2021. *Continuous monitoring of SO_2 emissions from Sinabung Volcano, Indonesia*. DOI: 10.5194/egusphere-egu21-3711, 2021.

Kunrat, S., Kern, C., Alfianti, H., and Lerner, A.H., 2022. Forecasting explosions at Sinabung Volcano, Indonesia, based on SO_2

emission rates. *Frontiers in Earth Science*, 10, p.1-15. DOI: 10.3389/feart.2022.976928.

Nakada, S., Zaennudin, A., Yoshimoto, M., Maeno, F., Suzuki, Y., Hokanishi, N., Sasaki, H., Iguchi, M., Ohkura, T., Gunawan, H., and Triastuty, H., 2019. Growth process of the lava dome/flow complex at Sinabung Volcano during 2013-2016. *Journal of Volcanology and Geothermal Research*, 382, p.120-136. DOI: 10.1016/j.jvolgeores.2017.06.012.

Optical Sensing, G., 2007. *Mobile DOAS Software Manual*, p.1-30.

Reath, K., Pritchard, M.E., Moruzzi, S., Alcott, A., Coppola, D., and Pieri, D., 2019. The AVTOD (ASTER Volcanic Thermal Output Database) Latin America archive, *Journal of Volcanology and Geothermal Research*, 376, p.62-74. DOI: 10.1016/j.jvolgeores.2019.03.019.

Rivera, A.M.M., 2011. Comparisons between OMI SO_2 data and ground- based SO_2 measurements at Turrialba Volcano, 92.

Rolim, S.B.A., Grondona, A., Hackmann, C.L., and Rocha, C., 2016. A Review of Temperature and Emissivity Retrieval Methods: Applications and Restrictions. *American Journal of Environmental Engineering*, 6 (4A), p.119-128. DOI: 10.5923/s.ajee.201601.18.

Saepuloh, A., Mirelva, P.R., and Wikantika, K., 2019. Advanced Applications of Synthetic Aperture Radar (SAR) Remote Sensing for Detecting Pre- and Syn-eruption Signatures at Mount Sinabung, North Sumatra, Indonesia. *Indonesian Journal on Geoscience*, 6 (2), p.123-140. DOI: 10.17014/ijog.6.2.123-140.

Saepuloh, A., Saputro, R.H., Heriawan, M.N., and Malik, D., 2020. Integration of Thermal Infrared and Synthetic Aperture Radar Images to Identify Geothermal Steam Spots Under Thick Vegetation Cover. *Natural Resources Research*, 30 (1), p.245-258. DOI: 0.1007/s11053-020-09754-9.

Shinohara, H., 2013. Volatile flux from subduction zone volcanoes: Insights from a detailed evaluation of the fluxes from volcanoes in japan. *Journal of Volcanology and Geothermal Research*. DOI: 10.1016/j.jvolgeores.2013.10.007.

Silvestri, M., Romaniello, V., Hook, S., Musacchio, M., Teggi, S., and Buongiorno, M.F. 2020. First comparisons of surface temperature estimations between ECOSTRESS, ASTER and landsat 8 over Italian volcanic and geothermal areas. *Remote Sensing*, 12 (1), p.1-11. DOI: 10.3390/RS12010184.

Suparman, Y., Afnimar, and Syahbana, D.K., 2021. The Drop of Relative Velocity Variation and Coherence Values Prior to Sinabung 2013 Eruptions. *Indonesian Journal on Geoscience*, 8 (1), p.109-117. DOI: 10.17014/ijog.8.1.109-117

Syahbana, D.K., Kasbani, K., Suantika, G., Prambada, O., Andreas, A.S., Saing, U.B., Kunrat, S.L., Andreastuti, S., Martanto, M., Kriswati, E., Suparman, Y., Humaida, H., Ogburn, S., Kelly, P.J., Wellik, J., Wright, H.M.N., Pesicek, J.D., Wessels, R., Kern, C., Lisowski, M., Diefenbach, A., Poland, M., Beauducel, F., Pallister, J., Vaughan, R.G., and Lowenstern, J.B., 2019. The 2017-19 activity at Mount Agung in Bali (Indonesia): Intense unrest, monitoring, crisis response, evacuation, and eruption. *Scientific Reports*, 9 (1). DOI: 10.1038/s41598-019-45295-9.

Symonds, R.B., Gerlach, T.M., and Reed, M.H., 2001. Magmatic gas scrubbing: Implications for volcano monitoring. *Journal of Volcanology and Geothermal Research*, 108 (1-4), p.303-341. DOI: 10.1016/S0377-0273(00)00292-4.

Textor, C., Graf, H.F., Timmreck, C., and Robock, A., 2004. *Emissions from volcanoes*, p.269-303. DOI: 10.1007/978-1-4020-2167-1_7.

Voigt, S., Orphal, J., Bogumil, K., and Burrows, J.P., 2001. The temperature dependence (203-293 K) of the absorption cross sections of O3in the 230-850 nm region measured by Fourier-transform spectroscopy, *Journal of Photochemistry and Photobiology A: Chemistry*, 143 (1), p.1-9. DOI: 10.1016/S1010-6030(01)00480-4.

Glasow, R., 2008. News & views. *Nature*, 453, p.1195-1196.

Zaennudin, A., 2011. Perbandingan antara erupsi Gunung Bromo Tahun 2010-2011 dan erupsi Kompleks Gunung Tengger. *Jurnal Lingkungan Dan Bencana Geologi*, 2 (1), p.21-37.